ACS APPLIED MATERIALS & INTERFACES

www.acsami.org

Research Article

Pre-Solid Electrolyte Interphase-Covered Li Metal Anode with Improved Electro-Chemo-Mechanical Reliability in High-Energy-Density Batteries

Xi Chen, Mingwei Shang, and Junjie Niu*

Cite This: *ACS Appl. Mater. Interfaces* 2021, 13, 34064−34073

Read Online

ACCESS | Metrics & More | Article Recommendations | Supporting Information

ABSTRACT: Mossy/dendritic lithium growth and infinite volume change lead to form an unstable solid electrolyte interphase (SEI) on the Li surface, thus resulting in poor cyclability in Li metal-based batteries. Design of a reliable SEI layer on Li metal is one of the promising strategies to reach high-energy-density lithium-ion batteries. In this article, we report a novel design of artificial pre-SEI-covered Li metal by using a facile drop-coating process which advances a highly reliable SEI formation with uniform Li plating/stripping, enabling a greatly increased cycling performance with high Coulombic efficiency in full-cell batteries. The electron-isolated organic polymer matrix provides elastic deformation that decreases the fracture failure, thus avoiding the crack during cycling. The formed metal−organic-salt LiCN through the precursor reaction with Li metal suffices a robust connection. In parallel, the homogeneous distribution of inorganic compounds ensures an enhanced ionic conductivity, which leads to a thinner, stable SEI layer by reducing electrolyte consumption and forming less dead lithium. As a result, the full-cell battery *versus* $LiNi_{0.8}Co_{0.15}Al_{0.05}O_2$ displayed a high capacity of 167.8 mA h g^{-1} after 100 cycles at 0.2 C in an electrolyte of 5.0 μL (mA h)$^{-1}$, while the battery with Li foil dropped to only 48.5 mA h g^{-1} after 65 cycles. The estimated energy density of the coin cell battery was about 404.8 W h kg^{-1} in the lean electrolyte of 1.25 μL (mA h)$^{-1}$. A high capacity retention over 84.0 and 81.0% and a Coulombic inefficiency less than 0.71 and 0.68% after 150 cycles with the 150 and 300 mA h pouch cell batteries paired with $LiNi_{0.5}Mn_{0.3}Co_{0.2}O_2$ (NMC532) were, respectively, achieved, which are much better than those of the batteries with Li foil. It is believed that the reinforced artificial pre-SEI covered on Li metal opens a new pathway to create a highly reliable, safe Li metal electrode for high energy-density batteries.

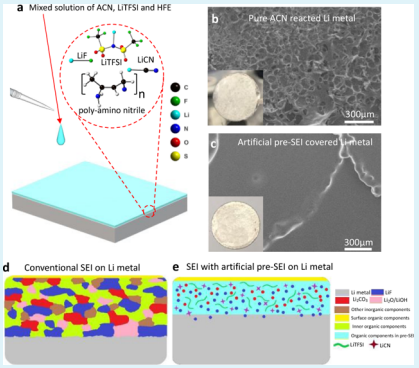

KEYWORDS: *Li metal anode, stable SEI, surface modification, high-energy density, lithium-ion batteries*

INTRODUCTION

Li metal, having almost 10 times higher capacity than graphite, is considered as one of the most promising anode electrodes for next-generation lithium-ion batteries which can deliver an energy density over 500 W h kg^{-1}.[1,2] One of the major barriers is the unreliable solid electrolyte interphase (SEI) layer on the Li surface which results in the fast performance failure as well as forming dendrites.[3,4] Due to the infinite volume change, continuous disappearing and generating SEI happen upon Li plating and stripping, which leads to large electrolyte consumption and active Li loss.[5] In addition, the traditional mosaic and multilayer SEI with the carbonate electrolyte shows non-uniformly dispersed inorganic and organic components,[6] resulting in a low ionic conductivity and a low mechanical strength.[7,8] The SEI can be modified by using advanced electrolytes and additives such as ether-based electrolytes,[9,10] molecular level solvent,[11] local high lithium salt concentrations,[12,13] lithium salt additives,[14] and single-ion conductive network.[15] Till date, several strategies in designing an artificial SEI on Li metal such as conductive material coatings[16−18] have been attempted.[19] It was found that the distribution of ionically conductive inorganic lithium compounds LiF[20−23] and Li_3N[24,25] plays an important role on stabilizing the SEI layer on Li metal.[26] A carbonate-based electrolyte additive fluoroethylene carbonate (FEC) can assist to form a stable SEI on the Li metal surface.[27,28] Recently an organic-rich SEI on polymer graphene oxide nanosheets showed improved battery performance even under low-temperature conditions.[29,30]

Here, we report a new pre-SEI strategy that advances to form a highly reliable SEI on the Li metal electrode. The artificial pre-SEI layer contains an organic polymer matrix filled with homogeneous lithium salts, which displayed reinforced mechanical property and enhanced electrochemical stability. An overpotential as low as 80 mV after 2000 h cycling under 3

Received: March 31, 2021
Accepted: July 7, 2021
Published: July 15, 2021

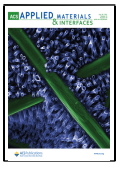

https://doi.org/10.1021/acsami.1c05966
ACS Appl. Mater. Interfaces 2021, 13, 34064−34073

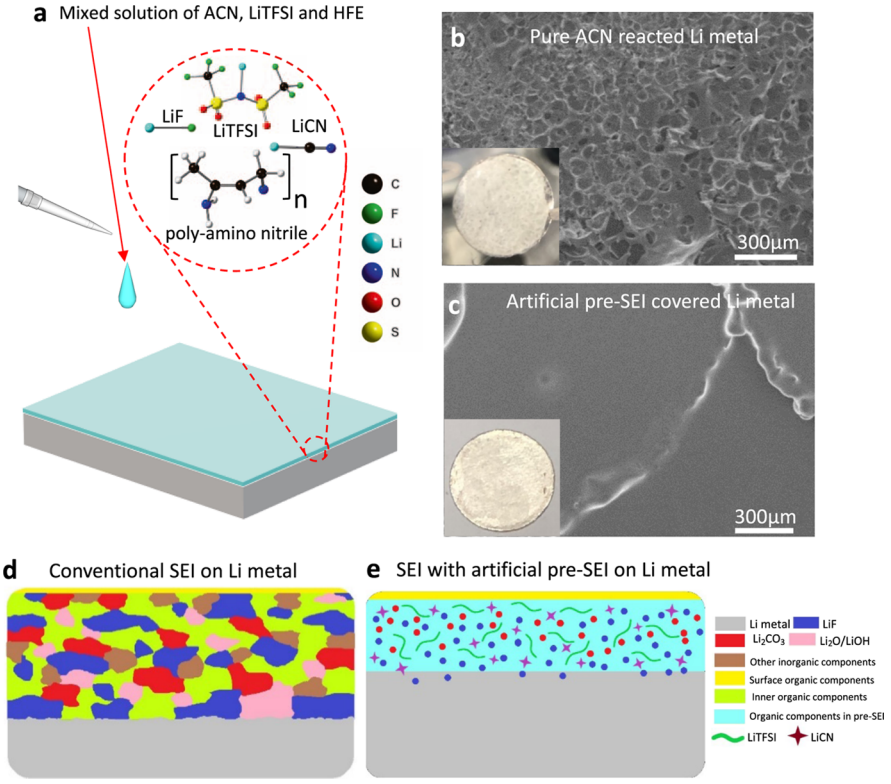

Figure 1. Process and structure of the reinforced artificial pre-SEI on Li metal. (a) Schematic graph of the drop-coating process. The surface structure of Li metal after reacting with pure ACN (b) and a mixed solution of 10.0 vol % ACN, 1.0 M LiTFSI, and 90.0 vol % HFE (c). Insets in (b,c) are the corresponding digital images. Anatomy of conventional SEI (d) and the SEI with pre-SEI (e) on Li metals.

mA cm^{-2} in symmetric cells was obtained, which was much better than Li foil that shorted in 300 h. Full coin cell batteries with high capacity retention and high energy density under lean electrolyte conditions were achieved. In parallel, a high capacity of as high as 242.9 mA h along with an average Coulombic inefficiency less than 0.68% after 150 cycles in full pouch cells was received.

RESULTS AND DISCUSSION

The artificial pre-SEI was developed on Li metal using a drop-coating method (Figure 1a). When the precursor solution of acetonitrile (ACN), 1,1,2,2-tetrafluoroethyl 2,2,2-trifluoroethyl ether (HFE), and lithium bis(trifluoromethanesulfonyl)imide (LiTFSI) was dropped on a Li metal surface, a series of reactions happened (Figure S1).[31] The major products include lithium cyanide (LiCN), LiF, methane, and organic poly-amino nitriles. ACN first reacted with Li to form ionically bonded lithium cyanide, which makes an intimate connection with Li metal. Following a series of successive reactions between the intermediate products and ACN, a long-chain poly-amino nitrile of poly-1,3-amino-1-methyl-4-nitrilebuta-1,3-diene was formed, which provides high flexibility to accommodate the volume variation during the Li plating/stripping. To mitigate the rigorous reaction and avoid void generation via methane bubbles (Figure 1b), a diluted ACN solution with HFE solvent and 1.0 M LiTFSI additive was applied.[32] The formed pre-SEI layer with ACN concentrations of 5.0 vol % (Figure S2a), 10.0 vol % (Figure 1c), and 20.0 vol % (Figure S2b) showed a greatly improved smooth surface, respectively.

The as-received pre-SEI layer was diagnosed using annular dark-field (ADF, Figure 2a) and bright-field (Figure S3a) scanning transmission electron microscopy (STEM). The corresponding energy dispersive X-ray spectra confirmed the uniform distribution of C, N, F, S, and O elements (Figures 2a and S3b–e). The lattice fringes of the high-resolution (HR) transmission electron microscopy (TEM) image revealed the presence of inorganic crystal domains of LiCN (210) and LiF (111)/(200) planes (Figure 2b). The components inside the pre-SEI were further investigated using electron energy loss spectroscopy (EELS). In contrast to conventional SEI, a much stronger and sharper Li K-edge peak at ~62 eV and a wide peak centered at 70 eV of the pre-SEI indicated the existence of more inorganic lithium compounds such as LiF.[33,34] The C K-edge peaks centered at about 286.8 and 295 eV are, respectively, regarded to the C−H and C═O bonds from the carbonate components in conventional SEI,[35] while a broad peak at 300 eV appeared in the pre-SEI, which could be related to the bonding of C≡N from the lithium cyanide (Figure 2d). An intensive N K-edge peak ranging from 400 to 420 eV mainly derives from the abundant organic amines and nitriles as well as cyanides (Figure 2e). The F K-edge peak between 691 and 695 eV of the pre-SEI further confirmed the fluorinated compounds from LiTFSI and HFE (Figure 2f).

The chemical composition of the pre-SEI was also characterized by using X-ray photoelectron spectroscopy (XPS). In the comparison to conventional SEI, as shown in Figure 2g, a strong C 1s peak at 286.8 eV and N 1s peaks at 397.9 and 400.5 eV demonstrated the presence of plenty of C−N/C≡N groups that originate from the products of the Li−ACN reaction (Figure 2h). The very strong C 1s peak at 290.4 eV and F 1s peak at 688.6 eV that correspond to C−F indicated the formation of fluorinated organic components in the pre-SEI. The C 1s peak at 293.3 eV and N 1s peak at 401.9

https://doi.org/10.1021/acsami.1c05966
ACS Appl. Mater. Interfaces 2021, 13, 34064−34073

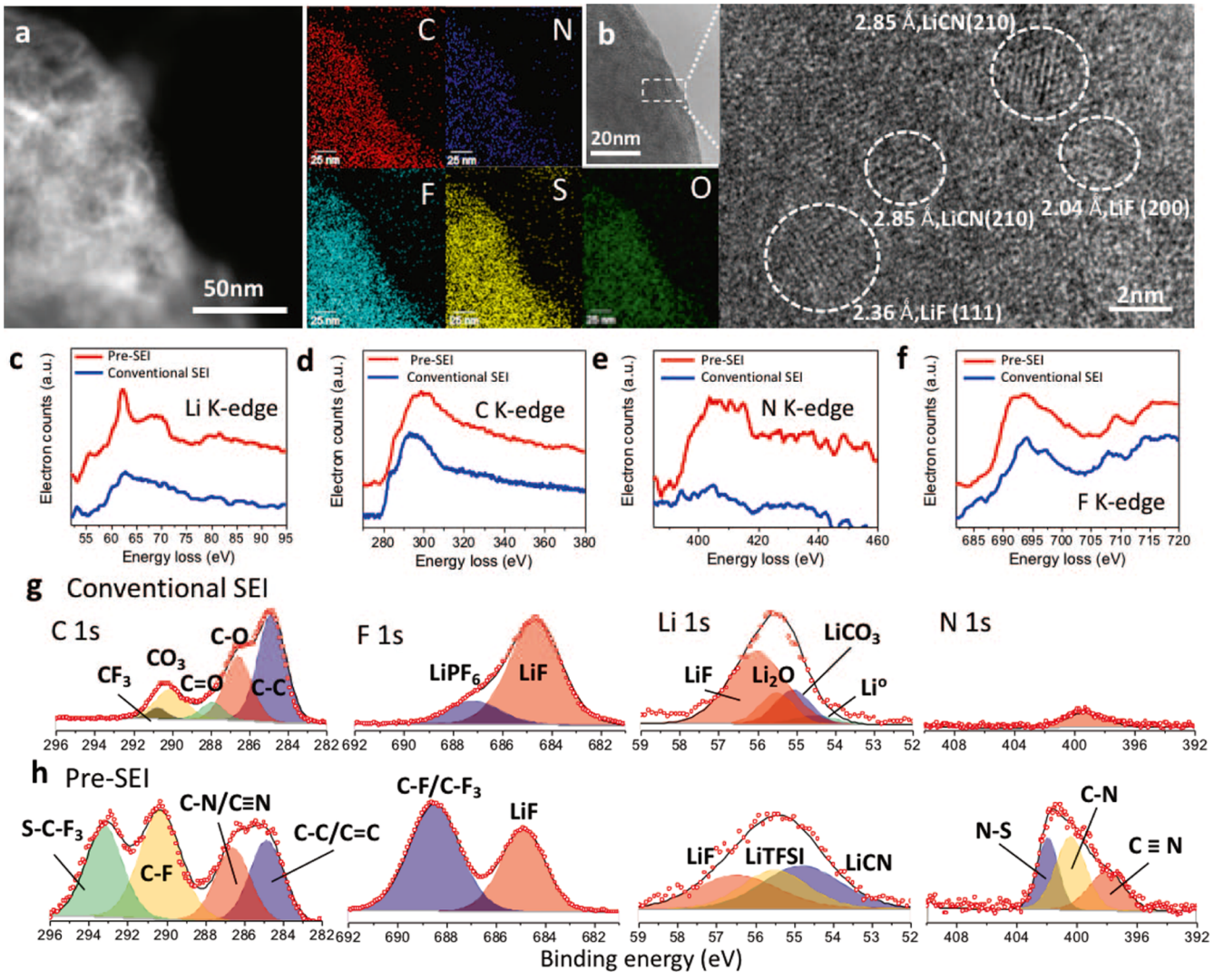

Figure 2. Morphology and chemical composition analysis of the artificial pre-SEI. (a) STEM ADF morphology and the corresponding element mappings of the pre-SEI on Li. (b) HRTEM image of the pre-SEI showing the lattice fringes of LiF and LiCN. (c–f) Li, C, N, and F K-edge EELS spectra of the pre-SEI. HR XPS spectra of C 1s, F 1s, Li 1s, and N 1s with the conventional SEI on Li metal in carbonate electrolyte (g) and the pre-SEI (h). The conventional SEI sample was collected after 24 h immersion in the electrolyte of 1.0 M $LiPF_6$ dissolved in a 3:7 weight ratio of EC and DEC without cycling. The pre-SEI sample was prepared by using a HFE solution with 10.0 vol % ACN and 1.0 M LiTFSI.

eV are both from the LiTFSI component. The F 1s peak at 684.8 eV and Li 1s peak at 56.4 eV revealed the generated LiF with both conventional SEI and pre-SEI samples. The appeared Li 1s peaks at 55.5 and 54.8 eV are from other lithium salts of LiTFSI and newly formed LiCN, respectively. The Fourier-transform infrared spectra revealed the existence of C−N, C═C, NH_2, and C≡N stretches in pure ACN reacted Li foil (Figure S4). Also, the XPS data of pure ACN on Li metal, as shown in Figure S5, exhibited C 1s peaks at 286.9 and 284.8 eV and N 1s peaks at 398.3 and 399.8 eV, which correspond to the C−C, C═C, C−N, and C≡N bondings, while the Li 1s peak at 54.8 eV confirmed the formation of LiCN. The XPS results of LiTFSI in ACN solution on Li metal showed peaks of C 1s at 290.1 and 293.2 eV, F 1s at 687.4 eV, N 1s at 401.9 eV, and Li 1s at 55.7 eV, which confirmed the existing LiTFSI (Figure S6). The new F 1s peak at 684.8 eV was from the LiF compound. In addition to the electrolyte decomposition, LiF was also formed by the reaction of HFE with Li metal, as shown from the peaks of F 1s at 684.8 eV and Li 1s at 56.2 eV (Figure S7). It was estimated that the layer thickness with C−F/C−F_3 groups was about 220−440 nm by applying long-time etching (Figure S8).

The composition distribution across the Li surface with and without pre-SEI after cycling in symmetric cells was, respectively, analyzed via XPS depth profiling. From the top surface to about 70.4 nm (160 s) depth, the high-intensity peaks of C 1s at 286.8/290.4 eV, N 1s at ∼400.5 eV, and the F 1s at 688.2 eV of the sample with pre-SEI indicated a constant distribution of the organic components inside the whole SEI layer (Figure 3). In parallel, the almost unchanged peak intensities of F 1s, Li 1s, and N 1s confirmed a uniformly dispersed inorganic compounds of LiCN, LiF, and LiTFSI across the SEI layer. As a comparison, the traditional SEI showed much less organic compounds, which were mostly concentrated on the top surface (Figure S9). Through the depth analysis, we found that the overall configuration and composition distribution of the SEI layer with pre-SEI-covered Li were not changed upon cycling, which demonstrated an electro-chemo-mechanically stable SEI formation.

https://doi.org/10.1021/acsami.1c05966
ACS Appl. Mater. Interfaces 2021, 13, 34064−34073

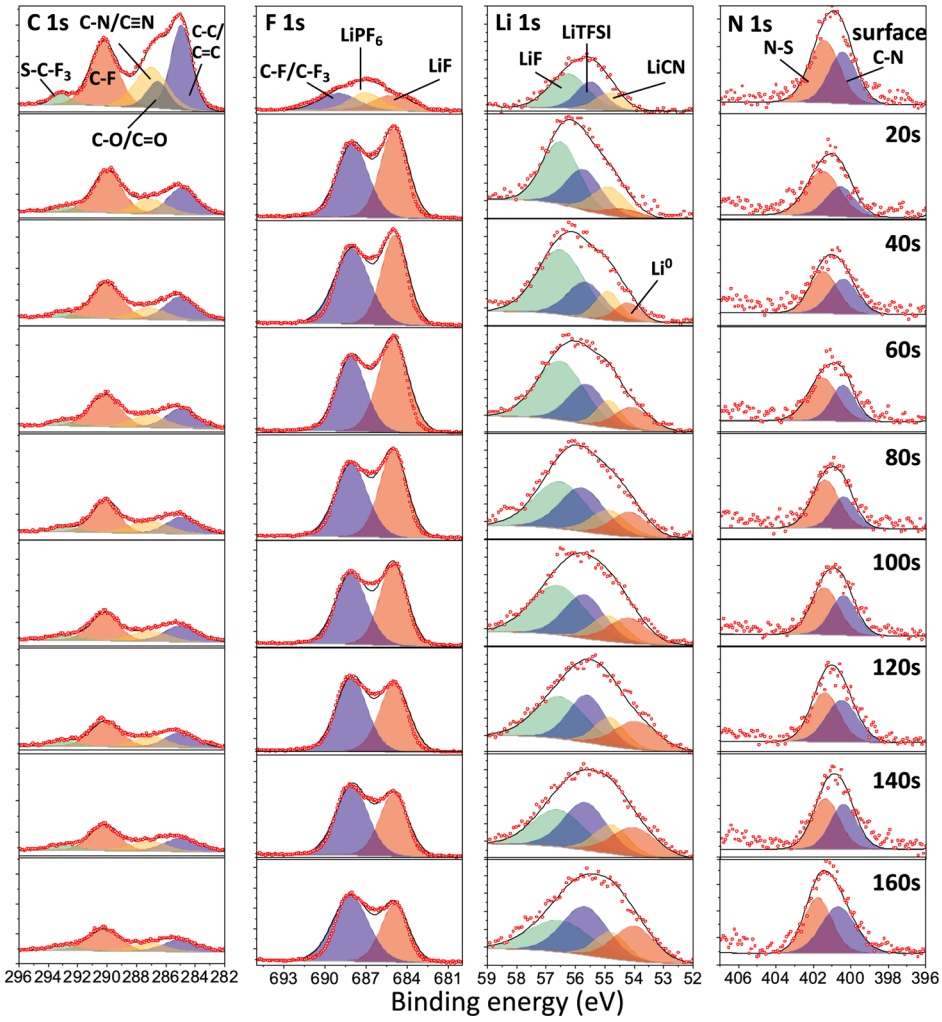

Figure 3. HR XPS spectra depth profiles of the pre-SEI-covered Li metal upon stripping after three cycles in symmetric cells. Electrolyte: 1.0 M $LiPF_6$ dissolved in a 3:7 weight ratio of EC and DEC. Current density: 1.0 mA cm^{-2}. Capacity: 1.0 mA h cm^{-2}.

On the basis of above diagnosis, the formed SEI with pre-SEI layer shows high potential in good mechanical flexibility from the organic compounds of poly-amino nitriles, better ionic conductivity from the homogeneous LiF and LiTFSI distribution, and tight connection with Li metal by forming LiCN (Figure 1b). Therefore, a robust, thinner SEI compared with conventional SEI can be formed, which will lead to an improved electro-chemo-mechanical stability with less electrolyte consumption.

Due to the low activation energy, uneven Li plating/stripping surface with mossy/dendritic lithium will form (Figure 4a). It was found that plenty of large irregular Li clusters were formed after plating (Figure 4b) and stripping (Figure 4c) on pure Li foil in symmetric cells. The root mean square height Sq was increased to 3.34 upon plating after 10 cycles (Figure 4l), compared to the Sq of 0.5 with pristine Li foil (Figure 4k). The pre-SEI-covered Li showed largely improved Li plating (Figure 4e) and stripping (Figure 4f) homogeneity under 1.0 mA cm^{-2} and 1.0 mA h cm^{-2}. Even under higher current densities of 3.0 and 5.0 mA cm^{-2} and capacities of 3.0 and 5.0 mA h cm^{-2}, a smooth surface upon plating (Figure 4g,i) and stripping (Figure 4h,j) was still obtained. The roughness Sq of the initial pre-SEI-covered Li is 0.56 (Figure 4m), which is similar to the pristine Li foil. After 10 cycles at 1.0 mA cm^{-2} and 1.0 mA h cm^{-2}, the roughness was slightly increased to 1.83 (Figure 4n) upon plating, which is almost half value of the Li foil. It is clear that the covered pre-SEI promoted the formation of a reliable SEI, enabling a uniform Li deposition and extraction even under high current densities.

Electrochemical stability of the pre-SEI-covered Li during Li plating and stripping was investigated under 3.0 mA cm^{-2} and 3.0 mA h cm^{-2} in symmetric cells (Figure 5a). The cell of pre-SEI-covered Li using 10.0 vol % ACN showed an overpotential of about ±100 mV at the initial 20 h (Figure 5b) and then stabilized at ±75 mV (Figure 5c,d) over 2000 h (1000 cycles). The cell with 20.0 vol % ACN displayed an initial overpotential of about ±200 mV and then stabilized at ±150 mV. The cell with Li foil had a low initial overpotential of about ±80−100 mV, while it rapidly raised to over ±400 mV after 300 h and reached a short-circuit. The presence of inorganic/organic components of the pre-SEI slightly increases the initial Li formation barrier due to the mitigated electronic conductivity that hikes the overpotential. While after a reliable SEI forming, the excellent electro-chemo-mechanical stability contributes to a smooth Li plating and stripping under a constant overpotential. However, irregular structures including mossy/dendritic Li are formed due to the rigorous growth on the highly conductive pure Li metal surface, which leads to a quick overpotential increase to short circuit. In this work, the pre-SEI

https://doi.org/10.1021/acsami.1c05966
ACS Appl. Mater. Interfaces 2021, 13, 34064−34073

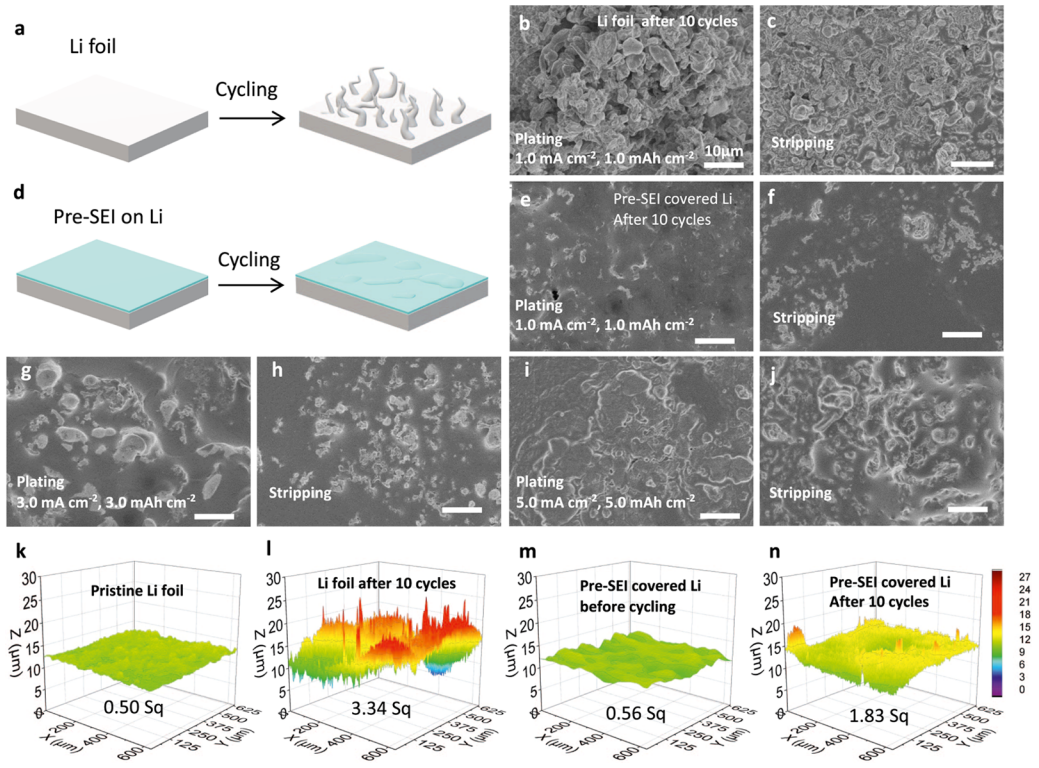

Figure 4. Surface morphology evolution of the Li metal with and without pre-SEI upon Li plating/stripping after 10 cycles in symmetric cells. Schematic (a) and SEM images of pure Li foil upon plating (b) and stripping (c) after 10 cycles under a current density of 1.0 mA cm^{-2} and capacity of 1.0 mA h cm^{-2}. Schematic (d) and SEM images of pre-SEI-covered Li upon plating (e,g,i) and stripping (f,h,j) after 10 cycles under current densities of 1.0, 3.0, and 5.0 mA cm^{-2} and capacities of 1.0, 3.0, and 5.0 mA h cm^{-2}, respectively. Scale bar: 10 μm. 3D confocal surface morphologies (600 × 600 μm) of pristine Li foil (k), Li foil upon plating after 10 cycles (l), pre-SEI-covered Li before (m), and after 10 cycles upon plating (n) at 1.0 mA cm^{-2}, 1.0 mA h cm^{-2}.

with a moderate 10.0 vol % ACN was applied for electrochemical battery studies. The symmetric cells also showed stable and low overpotential under a series of current densities from 0.5 to 5.0 mA cm^{-2} and capacities from 0.5 to 5.0 mA h cm^{-2} (Figure S10). The interfacial resistance was investigated by using Nyquist plots from electrochemical impedance spectroscopy (EIS) measurements in symmetric cells. The cell with pristine Li foil displayed a contact resistance of 10.2 Ω and a transfer resistance of 71.0 Ω (Figure 5e), while the cell with pre-SEI showed the resistance of 7.9 Ω and 91.4 Ω, respectively (Figure 5f). However, the charge-transfer resistance with Li foil was increased to 135.7 Ω after 100 cycles, whereas the value with pre-SEI was decreased to 69.7 Ω. The resistance variation upon cycling is in agreement with the overpotential evolution, as shown in Figure 5a−d. In addition, a sharp current jump after the first cycle of the Li foil in normal pulse voltammetry (NPV) measurements indicated a susceptible SEI layer under the pulse voltage, which may induce to form cracks (Figure 5g). The cell with pre-SEI exhibited a minor current change of ≤50 mA, which further demonstrated a good reliability even under a pulse voltage perturbation. To further investigate the Li plating/stripping reversibility under anode-free conditions, voltage profiles of CulLi symmetric cells with and without pre-SEI were collected after fully stripping Li from the Cu current collector under the limited electrolyte. As seen from Figure S11, the irreversible Li cycling of conventional Li foil appeared after only 60 h (30 cycles), with a drastic Coulombic efficiency (CE) drop from >90 to <10%. However, the cell with pre-SEI showed completely reversible cycling over 120 h (60 cycles) along with a high CE of over 90%.

Battery performance of full cells using the pre-SEI-covered Li (~30 μm) as the anode with an areal capacity of 6.18 mA h cm^{-2} and $LiNi_{0.8}Co_{0.15}Al_{0.05}O_2$ (NCA) as the cathode with an areal capacity of 3.92 mA h cm^{-2} was investigated under lean electrolyte conditions (Figure 6). It was found that the discharge capacity of the cell with Li foil dropped rapidly to 58.1 mA h g^{-1} (1.18 mA h cm^{-2}), 69.9 mA h g^{-1} (1.43 mA h cm^{-2}), and 117.3 mA h g^{-1} (2.40 mA h cm^{-2}) along with a low CE of 57.3, 78.3, and 96.8% after 20, 30, and 60 cycles under electrolyte amounts of 1.25, 2.5, and 5.0 μL mA h^{-1} [electrolyte to capacity, E/C ratio: 1.5, 3.0, and 6.0 g (A h)$^{-1}$], respectively (Figure 6a). This was due to the formation of an unstable, thick SEI layer by consuming plenty of the electrolyte on the electrode. After the Li metal anode was covered with pre-SEI, the battery showed a clearly improved cycling performance. As shown in Figure 6c, the cell with 10.0 vol % ACN still presented a capacity of 120.1, 130.2, and 167.9 mA h g^{-1} (2.46, 2.66, and 3.43 mA cm^{-2}), with a CE of 96.8, 96.2, and 99.2% after 40, 60, and 100 cycles, respectively. The capacity retention of the battery over 100 cycles with 5.0 μL (mA h)$^{-1}$ electrolyte was larger than 88.2% based on the initial capacity of 190.3 mA h g^{-1}. When the ACN concentration was increased to 20.0 vol %, the thicker pre-SEI layer increases the resistance, leading to a slightly reduced capacity retention upon cycling under different amounts of the electrolyte (Figure 6e). As seen from the corresponding voltage profiles with electrolyte of 5.0 μL (mA h)$^{-1}$ in Figure 6b,d,f, the battery with 10.0 vol % ACN showed a minimal capacity decay of less

https://doi.org/10.1021/acsami.1c05966
ACS Appl. Mater. Interfaces 2021, 13, 34064−34073

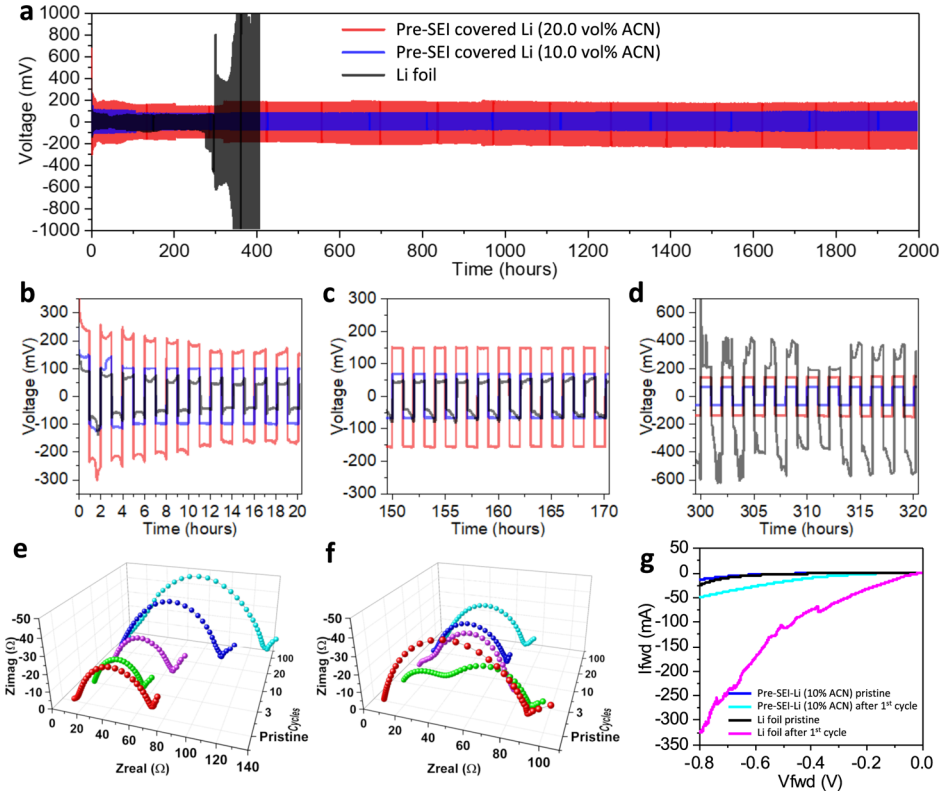

Figure 5. Electrochemical stability of the pre-SEI-covered Li metal. (a) Galvanostatic cycling of symmetric cells at 3.0 mA cm^{-2} and 3.0 mA h cm^{-2}. Red: 20.0 vol % ACN. Blue: 10.0 vol % ACN. Black: Li foil. The enlarged cycling profiles with the first 20 h (10 cycles) (b), 150−170 h (75−85 cycles) (c), and 300−320 h (150−160 cycles) (d), respectively. Nyquist plots of pure Li foil (e) and pre-SEI-covered Li (f) from EIS measurements in symmetric cells. (g) NPV curves of Li foil and pre-SEI-covered Li before and after the first cycle in symmetric cells.

than 5.8% after 50 cycles, which is much lower than the 12.9% drop of the cell with 20.0 vol % ACN and 25.3% drop of the cell with Li foil. Similar to the symmetric cells, as shown in Figure 5e,f, owing to the reliable SEI formation, the full cell with pre-SEI-covered Li displayed reduced both contact resistance and transfer resistance from 11.1 and 99.6 to 13.7 and 55.9 Ω after 50 cycles (Figure S12b), while the cell with Li foil exhibited an opposite trend (Figure S12a). The greatly improved stability of the SEI derived from the pre-SEI reduces the electrolyte consumption, which made the battery possible with a high energy density up to 404.8 W h kg^{-1} (Table S1).

Full pouch cells with total capacities of 150 and 300 mA h using five layers of pre-SEI-covered Li (three layers of double-side covered and two layers of single-side covered) as the anode *versus* four layers of double-side-coated NMC532 (areal capacity of 3.87 mA h cm^{-2}) as the cathode were, respectively, checked. Figure 7a demonstrates a running fan with a power of 2.5 W driven by the as-received 150 mA h pouch cell. Digital images of the coated cathode and the pre-SEI-covered Li metal anode for pouch cell assembly are shown in Figure 7b. The cross-section morphology in Figure 7c displays a sandwich geometry with a copper current collector in middle that was connected by two-sided pre-SEI-covered Li metal with a thickness of about 30−50 μm. In parallel, the sandwich configuration of the cathode was formed by applying an aluminum in middle and double-sided NMC532 layer with a thickness of ∼45 μm (areal loading: 24.2 mg cm^{-2}) (Figure 7d). The battery showed a reliable capacity of 125.9 mA h (Figure 7e) and 242.9 mA h (Figure 7f) after 150 cycles, respectively. As a comparison, the battery with Li foil exhibited a fast capacity decay from 146.0 and 284.3 mA h to only 78.4 and 8.9 mA h after 150 cycles, respectively. On the basis of initial capacity of 146.4 and 299.8 mA h after formation, the capacity retention was >84.0% (Figure 7g) and >81.0% (Figure 7h), while the battery with Li foil only showed the capacity retention of 53.7 and 3.0%, respectively. The average Coulombic inefficiency of the pouch cell with pre-SEI Li was 0.71% (Figure 7i) and 0.68% (Figure 7j) in the first 150 cycles, respectively, which were much lower than the values of 1.13 and 3.4% with Li foil. Based on the components including the electrode, electrolyte, current collector, package foils, and tabs, the estimated energy density of the assembled pouch cells was about 181.6 W h kg^{-1} with 150 mA h and about 193.3 W h kg^{-1} with 300 mA h, respectively (Table S2).

A highly stable, safe Li metal electrode requires a reliable SEI layer that has both high elastic deformation and high ionic conductivity. In the pre-SEI design, the introduced organic polymer poly-amino nitrile serves as the base matrix, which provides sufficient mechanical flexibility to regulate the rigorous volume fluctuation of lithium upon deposition and extraction. Also, the generated lithium organic salt LiCN as a bridge ensures a strong connection with Li metal. The plenty of pre-formed, nanostructured inorganic/organic salts of LiF, LITFSI, and LiCN with uniform distribution effectively enhanced the Li^+ conductivity, while the electronic conductivity is largely reduced due to the existing polymer matrix and more inorganic compounds. As the result, an electro-chemo-mechanically stable SEI layer with less thickness due to the suppressed decomposition of electrolyte is formed, enabling a reversible, homogeneous Li plating and stripping.

https://doi.org/10.1021/acsami.1c05966
ACS Appl. Mater. Interfaces 2021, 13, 34064−34073

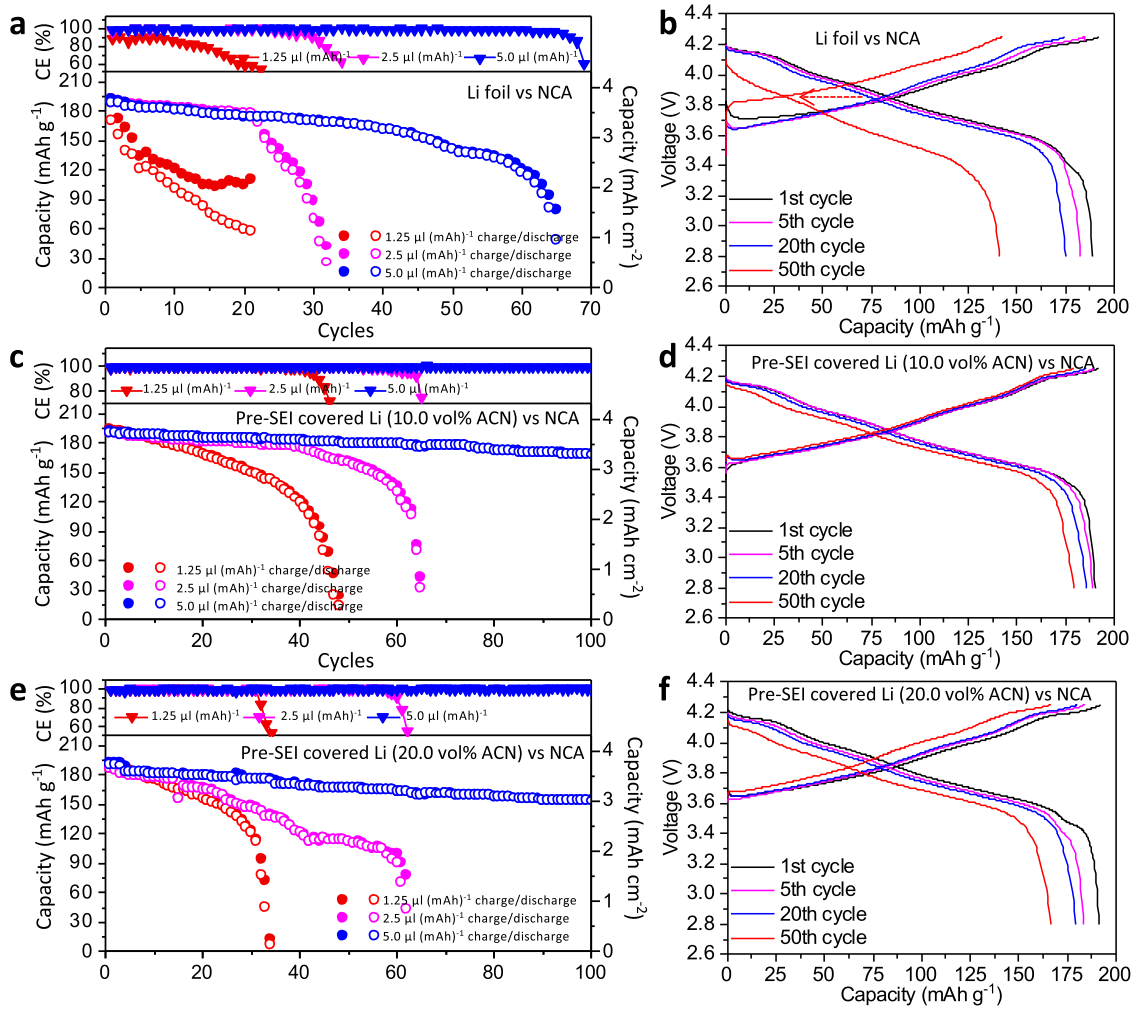

Figure 6. Battery performance of full cells under lean electrolyte conditions. Cycling capability and CE of full batteries of Li foil *vs* NCA (a), pre-SEI-covered Li *vs* NCA with 10.0 vol % ACN (c) and 20.0 vol % ACN (e) at 0.2 C by using the lean electrolyte of 1.25, 2.5, and 5.0 μL (mA h)$^{-1}$, respectively. (b,d,f) Corresponding voltage profiles at 1st, 5th, 20th, and 50th cycles with an electrolyte of 5.0 μL (mA h)$^{-1}$. The areal capacity of the anode is 6.18 mA h cm^{-2}. The loading and areal capacity of the NCA cathode are 20.5 mg cm^{-2} and 3.92 mA h cm^{-2}, respectively.

By applying the pre-SEI-covered Li metal as the electrode, a battery with improved cyclability and reduced dendrite risk can be achieved.

CONCLUSIONS

In summary, a pre-SEI-covered Li metal was designed by using a simple, mass-production available drop-coating process. The improved ionic conductivity, flexibility, and electron isolation due to the polymer network and plenty of lithium salts lead to form a thin SEI layer with improved electro-chemo-mechanical reliability. Highly reversible, uniform Li deposition and exaction with low risk of forming mossy-dendritic lithium even under high current densities were achieved, which contributed to a high-energy-density battery with long cycling performance. In symmetric cells, a low overpotential of 75 mV was received after 2000 h cycling under 3.0 mA cm^{-2}. The full cell batteries paired with NCA showed clearly improved cycling capability compared to Li foil under lean electrolyte conditions. The estimated initial energy density of the coin cell battery was about 404.8, 360.9, and 268.5 W h kg^{-1} with an *E*/*C* ratio of 1.5, 3.0, and 6.0 g (A h)$^{-1}$, respectively. In addition, pouch cells with high capacities of 242.9 and 125.9 mA h along with high capacity retention up to 84.0 and 81.0% over 150 cycles were, respectively, achieved. The current pre-SEI on Li metal displays high potential in various high-energy-density batteries that need reliable, safe Li metal as the electrode.

EXPERIMENTAL DETAILS

Preparation of Pre-SEI-Covered Li Metal. A Li foil with a thickness of ~100 μm (99.9% purity, Goodfellow) was polished by brass brush to remove the surface impurities. Then, the thickness was further reduced by applying a rolling process (Shenzhen Bonapu). 1.0 M lithium bis-trifluoromethane sulfonimide (99.95% purity, BASF Corp.) was dissolved in ACN solution (HPLC grade, >99.9%, Sigma-Aldrich). The received solution with different ACN concentrations of 5.0, 10.0, and 20.0 vol % was then mixed with HFE, respectively. The as-obtained precursor solution was used to form the pre-SEI on Li metal. In a typical experiment, 30 μL of precursor solution with 10.0 vol % ACN was drop-coated on a treated Li metal with a diameter of 1.56 cm (precursor solution loading: ~15.7 μL cm^{-2}). Subsequently, the sample was kept at room temperature overnight. For the reactions with pure ACN, 1.0 M LiTFSI ACN solution, and pure HFE, 60 μL of precursor mixture solution was, respectively, dropped on a Li foil and then was kept at room temperature overnight. All experiments were conducted inside an argon-filled glovebox (H_2O: <0.5 ppm, O_2: <0.1 ppm, LABstar^{pro}, MBraun).

Characterizations of the Samples. Scanning electron microscopy (SEM) characterization was conducted using a Hitachi S4800

https://doi.org/10.1021/acsami.1c05966
ACS Appl. Mater. Interfaces 2021, 13, 34064−34073

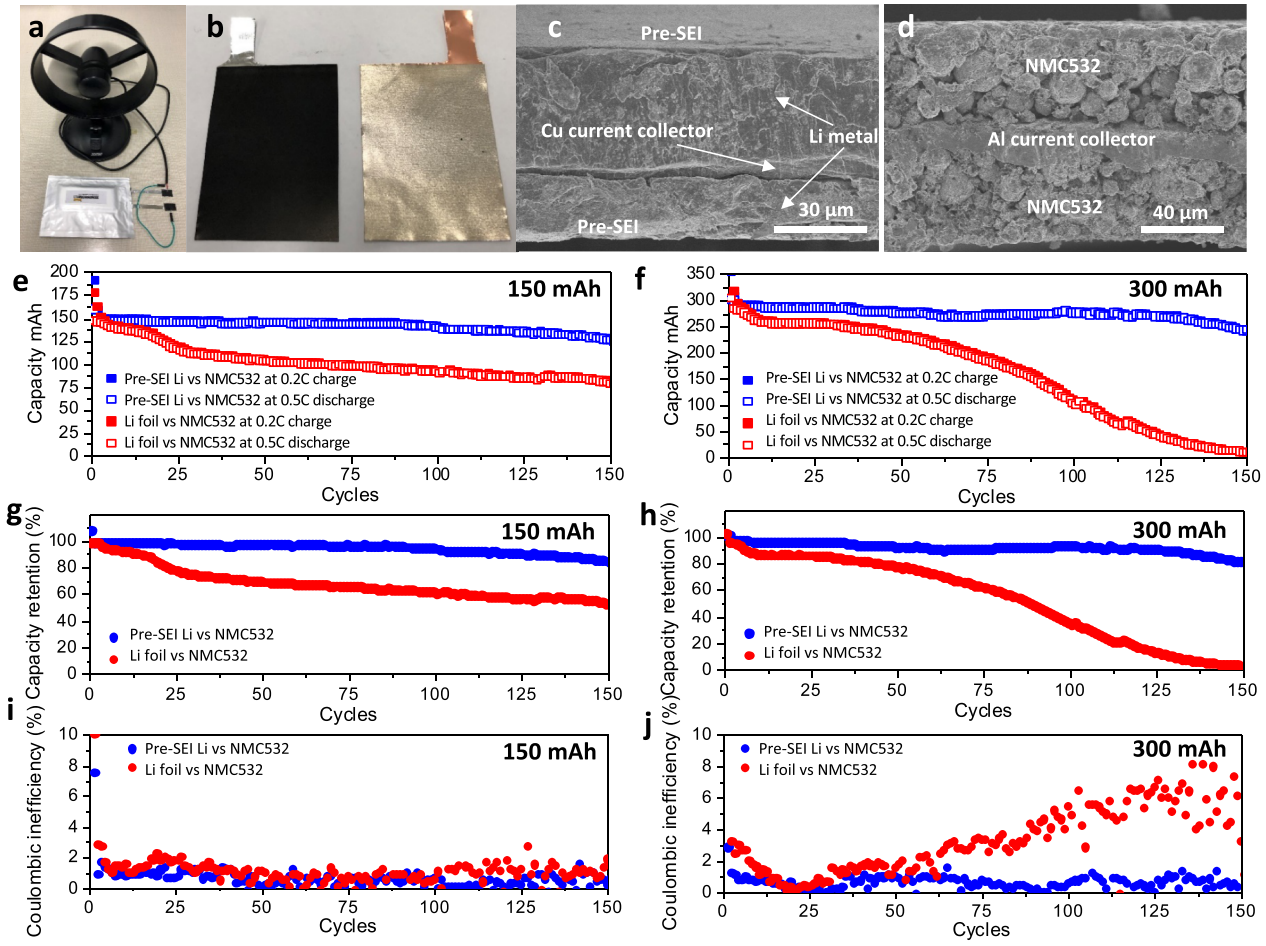

Figure 7. Battery performance of 150 and 300 mA h pouch cells. (a) Demonstration of a running 2.5 W fan powered by the 150 mA h pouch cell battery. (b) NMC532 cathode (left) and the pre-SEI-covered Li metal anode (right) for pouch cell assembly. SEM cross-section images of the pre-SEI double-side covered anode electrode (c) and the NMC532 double-side covered cathode electrode (d). Battery cycling performance (e,f), discharge capacity retention (g,h), and Coulombic inefficiency (i,j) of the pouch cells using pre-SEI-covered Li metal as the anode and NMC532 as the cathode with total capacities of 150 and 300 mA h, respectively. The pouch cells were assembled with five layers of pre-SEI-covered Li on Cu as the anode and four layers of double-side NMC-coated Al as the cathode.

ultra-HR field emission scanning electron microscope equipped with energy-dispersive X-ray spectroscopy (EDS). Surface morphology evolution of the Li metal was checked with various current densities after 10 cycles in symmetric coin cells. All samples were carefully rinsed with dimethyl ether (DME) to remove the electrolyte residuals before the characterization. HR-STEM images and EDS element mappings were operated on a JEOL JEM-ARM200CF 200 kV STEM/TEM, which was equipped with a probe aberration corrector. TEM images were performed under 200 kV accelerating voltage. ADF-STEM mode imaging and EDS element mappings were operated under 200 kV accelerating voltage with an image resolution of less than 0.08 nm and energy resolution of 0.35 eV. The EELS spectra were acquired under 0.25 eV/Ch and 5 mm aperture in high-loss EELS spectrum from 250 to 750 eV for C K-edge and N K-edge, 0.125 eV/Ch and 2.5 mm aperture in high-loss from 50 to 300 eV for Li K-edge, and 550 to 800 eV for F K-edge. The both pre-SEI-covered Li and conventional Li foil samples were sealed in an argon-filled container. The sample was exposed in air with less than 1 min before being transferred into the TEM chamber. XPS measurements were carried out at Thermo Scientific ESCALAB 250Xi XPS, which is affiliated with a scanning ion gun and an electron flood gun. A non-monochromatic X-ray of Al Kα line (a photon energy of 1486.6 eV) was irradiated at the sample. The spectra were collected using an ultrahigh vacuum instrument with a pressure below 1×10^{-10} Pa. The emitted electrons were detected using a hemispherical analyzer under an angle of 45° to the surface normal. All XPS spectra were fitted with Gaussian−Lorentzian functions and a Shirley-type background and plotted as a function of the binding energy with respect to the Fermi level. All the data were calibrated using the C 1s peak at 284.8 eV. 3D surface roughness was checked using Olympus LEXT OLS4100 3D laser confocal microscopy equipped with a 405 nm semiconductor laser photomultiplier detector.

Coin Cell Assembly. Symmetric cells (CR2032) were assembled by using the pre-SEI Li or Li foil as both anode and cathode. The electrolyte was 1.0 M LiTFSI in 1,3-dioxolane/DME with a 1:1 volume ratio and 0.1 M $LiNO_3$ as an additive. For the full coin cells (CR2032), the as-received pre-SEI Li or Li foil was directly used as the anode electrode without the slurry-mixing process. The cathode slurry was prepared by mixing 94 wt % NMC532 as active material, 4 wt % conductive carbon black (SuperP C65, Timcal), and 2 wt % poly(vinylidene fluoride) (average Mn ∼ 71,000, Sigma-Aldrich) as the binder in *N*-methyl-2-pyrrolidinone solution (Sigma-Aldrich). The mixed slurry was coated onto a 0.15 mm thick aluminum foil with an active material loading of 12.1 mg cm^{-2} until dried at 80 °C for 24 h in a vacuum oven. The NCA as cathode material was obtained from a brand-new 18650 Samsung 35E battery with an active material loading of 20.45 mg cm^{-2}. The cell was assembled using 1.0 M $LiPF_6$ dissolved in a 3:7 weight ratio of ethylene carbonate (EC) and diethylene carbonate (EMC) with 2 wt % vinylene carbonate (VC) and 10 wt % FEC as electrolytes. The symmetric cells with pre-SEI-covered Li and Li foil for XPS depth profiles were assembled using a FEC-free electrolyte of 1.0 M $LiPF_6$ dissolved in EC and diethyl

https://doi.org/10.1021/acsami.1c05966
ACS Appl. Mater. Interfaces 2021, 13, 34064−34073

carbonate (DEC) (1:1 volume ratio, LP47, BASF Corp.). A Celgard 2400 microporous polyethylene (PE) membrane was applied as the separator. All cells were assembled inside the argon-filled glovebox.

Pouch Cell Assembly. Full pouch cells with total capacities of 150 and 300 mA h were, respectively, assembled using five layers of pre-SEI-covered Li (three layers of double-side covered and two layers of single-side covered) as the anode *versus* four layers of double-side-coated NMC532 (areal capacity of 3.87 mA h cm^{-2}) as the cathode. The Celgard 2400 microporous PE membrane was used as the separator. The pre-SEI-covered Li or Li foil (China Energy Lithium Co. Ltd.) with a thickness of about 30−50 μm was contacted on a copper foil as the current collector. The Li areal loading was about 12.4 mA h cm^{-2}. The NMC532 areal loading was about 24.2 mg cm^{-2}. The Ni and Al tabs with 4 mm width were used for anode and cathode connections via an ultrasonic metal spot welding machine (TMAX Battery Equipment), respectively. The electrolyte used in pouch cells was 1.0 M $LiPF_6$ in a 3:7 weight ratio of EC and EMC with 2 wt % VC and 10 wt % FEC. The electrolyte amount was 6.0 g $(A\ h)^{-1}$ on the basis of cathode capacity. The cells were sealed using a pouch-cell vacuum sealing machine (TMAX Battery Equipment).

Electrochemical Property and Battery Performance Measurements. The EIS measurements were checked by Gamry 600+ Potentiostat/Galvanostat/ZRA. All the Li plating/stripping and battery cycling performance at different current densities was conducted using the galvanostatic charging/discharging method on a battery tester system (LANDT 2001CT, Landt Instruments, Inc.). The as-prepared full coin cells and full pouch cells were pre-activated under 0.1 C before cycling with a charge rate of 0.2 C and a discharge rate of 0.5 C. The anode-free cycling measurement was conducted via a symmetric cell that consists of a pre-SEI-covered Li on Cu as one electrode and a Li foil on Cu as the counter electrode. The anode-free electrode was obtained after completely stripping the lithium from the pre-SEI-covered Li electrode under a current density of 1.0 mA cm^{-2} and a cut-off voltage of 1.0 V. Then, the lithium plating process started under 3.0 mA cm^{-2} and 3.0 mA h cm^{-2}. A total 60 μL of electrolyte of 1.0 M $LiPF_6$ in EC and DEC (weight ratio 30:70) solvent was used.

■ ASSOCIATED CONTENT

Supporting Information

The Supporting Information is available free of charge at https://pubs.acs.org/doi/10.1021/acsami.1c05966.

Additional characterization and performance (PDF)

■ AUTHOR INFORMATION

Corresponding Author

Junjie Niu − *Department of Materials Science and Engineering, CEAS, University of Wisconsin-Milwaukee, Milwaukee, Wisconsin 53211, United States;* orcid.org/0000-0003-0093-7357; Email: niu@uwm.edu

Authors

Xi Chen − *Department of Materials Science and Engineering, CEAS, University of Wisconsin-Milwaukee, Milwaukee, Wisconsin 53211, United States;* orcid.org/0000-0002-3903-6540

Mingwei Shang − *Department of Materials Science and Engineering, CEAS, University of Wisconsin-Milwaukee, Milwaukee, Wisconsin 53211, United States*

Complete contact information is available at: https://pubs.acs.org/10.1021/acsami.1c05966

Author Contributions

J.N. and X.C. conceived the project. X.C. synthesized the samples and performed the characterizations and battery performance tests. M.S. performed XPS characterizations. X.C and J.N. wrote the manuscript. All authors analyzed the data and contributed to the discussion.

Notes

The authors declare no competing financial interest.

■ ACKNOWLEDGMENTS

Materials synthesis and battery tests were performed at the University of Wisconsin-Milwaukee (UWM). XRD and 3D confocal microscopy characterizations were carried out at the Advanced Analysis Facility (AAF), UWM. SEM was carried out at the UWM Biology Department Electron Microscopy Laboratory. Atomic resolution STEM imaging with EDS mappings and high-resolution XPS were performed at the facility of NUANCE Center at Northwestern University. X.C. thanks Dr. Bangxing Li for thoughtful discussion. All authors acknowledge the supports from the NSF grant #2013525, UW System Ignite Grant Program under award #FY21-Y-106-068000-4.

■ REFERENCES

(1) Albertus, P.; Babinec, S.; Litzelman, S.; Newman, A. Status and Challenges in Enabling the Lithium Metal Electrode for High-Energy and Low-Cost Rechargeable Batteries. *Nat. Energy* **2018**, *3*, 16−21.

(2) Liu, J.; Bao, Z.; Cui, Y.; Dufek, E. J.; Goodenough, J. B.; Khalifah, P.; Li, Q.; Liaw, B. Y.; Liu, P.; Manthiram, A.; Meng, Y. S.; Subramanian, V. R.; Toney, M. F.; Viswanathan, V. V.; Whittingham, M. S.; Xiao, J.; Xu, W.; Yang, J.; Yang, X.-Q.; Zhang, J.-G. Pathways for Practical High-Energy Long-Cycling Lithium Metal Batteries. *Nat. Energy* **2019**, *4*, 180−186.

(3) Xu, W.; Wang, J.; Ding, F.; Chen, X.; Nasybulin, E.; Zhang, Y.; Zhang, J.-G. Lithium Metal Anodes for Rechargeable Batteries. *Energy Environ. Sci.* **2014**, *7*, 513−537.

(4) Lin, D.; Liu, Y.; Cui, Y. Reviving the Lithium Metal Anode for High-Energy Batteries. *Nat. Nanotechnol.* **2017**, *12*, 194−206.

(5) Fang, C.; Li, J.; Zhang, M.; Zhang, Y.; Yang, F.; Lee, J. Z.; Lee, M.-H.; Alvarado, J.; Schroeder, M. A.; Yang, Y.; Lu, B.; Williams, N.; Ceja, M.; Yang, L.; Cai, M.; Gu, J.; Xu, K.; Wang, X.; Meng, Y. S. Quantifying Inactive Lithium in Lithium Metal Batteries. *Nature* **2019**, *572*, 511−515.

(6) Li, Y.; Li, Y.; Pei, A.; Yan, K.; Sun, Y.; Wu, C.-L.; Joubert, L.-M.; Chin, R.; Koh, A. L.; Yu, Y.; Perrino, J.; Butz, B.; Chu, S.; Cui, Y. Atomic Structure of Sensitive Battery Materials and Interfaces Revealed by Cryo−Electron Microscopy. *Science* **2017**, *358*, 506−510.

(7) Shen, X.; Zhang, R.; Chen, X.; Cheng, X.-B.; Li, X.; Zhang, Q. The Failure of Solid Electrolyte Interphase on Li Metal Anode: Structural Uniformity or Mechanical Strength? *Adv. Energy Mater.* **2020**, *10*, 1903645.

(8) Yu, Z.; Cui, Y.; Bao, Z. Design Principles of Artificial Solid Electrolyte Interphases for Lithium-Metal Anodes. *Cell Rep. Phys. Sci.* **2020**, *1*, 100119.

(9) Jiao, S.; Ren, X.; Cao, R.; Engelhard, M. H.; Liu, Y.; Hu, D.; Mei, D.; Zheng, J.; Zhao, W.; Li, Q.; Liu, N.; Adams, B. D.; Ma, C.; Liu, J.; Zhang, J.-G.; Xu, W. Stable Cycling of High-Voltage Lithium Metal Batteries in Ether Electrolytes. *Nat. Energy* **2018**, *3*, 739−746.

(10) Amanchukwu, C. V.; Yu, Z.; Kong, X.; Qin, J.; Cui, Y.; Bao, Z. A New Class of Ionically Conducting Fluorinated Ether Electrolytes with High Electrochemical Stability. *J. Am. Chem. Soc.* **2020**, *142*, 7393−7403.

(11) Yu, Z.; Wang, H.; Kong, X.; Huang, W.; Tsao, Y.; Mackanic, D. G.; Wang, K.; Wang, X.; Huang, W.; Choudhury, S.; Zheng, Y.; Amanchukwu, C. V.; Hung, S. T.; Ma, Y.; Lomeli, E. G.; Qin, J.; Cui, Y.; Bao, Z. Molecular Design for Electrolyte Solvents Enabling Energy-Dense and Long-Cycling Lithium Metal Batteries. *Nat. Energy* **2020**, *5*, 526−533.

(12) Chen, S.; Zheng, J.; Mei, D.; Han, K. S.; Engelhard, M. H.; Zhao, W.; Xu, W.; Liu, J.; Zhang, J.-G. High-Voltage Lithium-Metal Batteries Enabled by Localized High-Concentration Electrolytes. *Adv. Mater.* **2018**, *30*, 1706102.
(13) Wang, J.; Yamada, Y.; Sodeyama, K.; Chiang, C. H.; Tateyama, Y.; Yamada, A. Superconcentrated Electrolytes for a High-Voltage Lithium-Ion Battery. *Nat. Commun.* **2016**, *7*, 12032.
(14) Zheng, J.; Engelhard, M. H.; Mei, D.; Jiao, S.; Polzin, B. J.; Zhang, J.-G.; Xu, W. Electrolyte Additive Enabled Fast Charging and Stable Cycling Lithium Metal Batteries. *Nat. Energy* **2017**, *2*, 17012.
(15) Yu, Z.; Mackanic, D. G.; Michaels, W.; Lee, M.; Pei, A.; Feng, D.; Zhang, Q.; Tsao, Y.; Amanchukwu, C. V.; Yan, X.; Wang, H.; Chen, S.; Liu, K.; Kang, J.; Qin, J.; Cui, Y.; Bao, Z. A Dynamic, Electrolyte-Blocking, and Single-Ion-Conductive Network for Stable Lithium-Metal Anodes. *Joule* **2019**, *3*, 2761−2776.
(16) Zheng, G.; Lee, S. W.; Liang, Z.; Lee, H.-W.; Yan, K.; Yao, H.; Wang, H.; Li, W.; Chu, S.; Cui, Y. Interconnected Hollow Carbon Nanospheres for Stable Lithium Metal Anodes. *Nat. Nanotechnol.* **2014**, *9*, 618−623.
(17) Kim, M. S.; Ryu, J.-H.; Deepika; Lim, Y. R.; Nah, I. W.; Lee, K.-R.; Archer, L. A.; Il Cho, W. Langmuir−Blodgett Artificial Solid-Electrolyte Interphases for Practical Lithium Metal Batteries. *Nat. Energy* **2018**, *3*, 889−898.
(18) Chen, X.; Shang, M.; Niu, J. Inter-Layer-Calated Thin Li Metal Electrode with Improved Battery Capacity Retention and Dendrite Suppression. *Nano Lett.* **2020**, *20*, 2639−2646.
(19) Tu, Z.; Choudhury, S.; Zachman, M. J.; Wei, S.; Zhang, K.; Kourkoutis, L. F.; Archer, L. A. Designing Artificial Solid-Electrolyte Interphases for Single-Ion and High-Efficiency Transport in Batteries. *Joule* **2017**, *1*, 394−406.
(20) Cao, X.; Ren, X.; Zou, L.; Engelhard, M. H.; Huang, W.; Wang, H.; Matthews, B. E.; Lee, H.; Niu, C.; Arey, B. W.; Cui, Y.; Wang, C.; Xiao, J.; Liu, J.; Xu, W.; Zhang, J.-G. Monolithic Solid−Electrolyte Interphases Formed in Fluorinated Orthoformate-Based Electrolytes Minimize Li Depletion and Pulverization. *Nat. Energy* **2019**, *4*, 796−805.
(21) Pathak, R.; Chen, K.; Gurung, A.; Reza, K. M.; Bahrami, B.; Pokharel, J.; Baniya, A.; He, W.; Wu, F.; Zhou, Y.; Xu, K.; Qiao, Q. Fluorinated Hybrid Solid-Electrolyte-Interphase for Dendrite-Free Lithium Deposition. *Nat. Commun.* **2020**, *11*, 93.
(22) Suo, L.; Xue, W.; Gobet, M.; Greenbaum, S. G.; Wang, C.; Chen, Y.; Yang, W.; Li, Y.; Li, J. Fluorine-Donating Electrolytes Enable Highly Reversible 5-V-Class Li Metal Batteries. *Proc. Natl. Acad. Sci. U.S.A.* **2018**, *115*, 1156−1161.
(23) Cui, C.; Yang, C.; Eidson, N.; Chen, J.; Han, F.; Chen, L.; Luo, C.; Wang, P.-F.; Fan, X.; Wang, C. A Highly Reversible, Dendrite-Free Lithium Metal Anode Enabled by a Lithium-Fluoride-Enriched Interphase. *Adv. Mater.* **2020**, *32*, 1906427.
(24) Zhu, Y.; He, X.; Mo, Y. Strategies Based on Nitride Materials Chemistry to Stabilize Li Metal Anode. *Adv. Sci.* **2017**, *4*, 1600517.
(25) Li, Y.; Sun, Y.; Pei, A.; Chen, K.; Vailionis, A.; Li, Y.; Zheng, G.; Sun, J.; Cui, Y. Robust Pinhole-Free Li_3N Solid Electrolyte Grown from Molten Lithium. *ACS Cent. Sci.* **2018**, *4*, 97−104.
(26) Huang, W.; Wang, H.; Boyle, D. T.; Li, Y.; Cui, Y. Resolving Nanoscopic and Mesoscopic Heterogeneity of Fluorinated Species in Battery Solid-Electrolyte Interphases by Cryogenic Electron Microscopy. *ACS Energy Lett.* **2020**, *5*, 1128−1135.
(27) Markevich, E.; Salitra, G.; Chesneau, F.; Schmidt, M.; Aurbach, D. Very Stable Lithium Metal Stripping−Plating at a High Rate and High Areal Capacity in Fluoroethylene Carbonate-Based Organic Electrolyte Solution. *ACS Energy Lett.* **2017**, *2*, 1321−1326.
(28) Brown, Z. L.; Jurng, S.; Nguyen, C. C.; Lucht, B. L. Effect of Fluoroethylene Carbonate Electrolytes on the Nanostructure of the Solid Electrolyte Interphase and Performance of Lithium Metal Anodes. *ACS Appl. Energy Mater.* **2018**, *1*, 3057−3062.
(29) Gao, Y.; Rojas, T.; Wang, K.; Liu, S.; Wang, D.; Chen, T.; Wang, H.; Ngo, A. T.; Wang, D. Low-Temperature and High-Rate-Charging Lithium Metal Batteries Enabled by an Electrochemically Active Monolayer-Regulated Interface. *Nat. Energy* **2020**, *5*, 534−542.
(30) Shadike, Z.; Lee, H.; Borodin, O.; Cao, X.; Fan, X.; Wang, X.; Lin, R.; Bak, S.-M.; Ghose, S.; Xu, K.; Wang, C.; Liu, J.; Xiao, J.; Yang, X.-Q.; Hu, E. Identification of LiH and Nanocrystalline LiF in the Solid−Electrolyte Interphase of Lithium Metal Anodes. *Nat. Nanotechnol.* **2021**, *16*, 549−554.
(31) Rupich, M. W.; Pitts, L.; Abraham, K. M. Characterization of Reactions and Products of the Discharge and Forced Overdischarge of Li/SO_2 Cells. *J. Electrochem. Soc.* **1982**, *129*, 1857.
(32) Yamada, Y.; Furukawa, K.; Sodeyama, K.; Kikuchi, K.; Yaegashi, M.; Tateyama, Y.; Yamada, A. Unusual Stability of Acetonitrile-Based Superconcentrated Electrolytes for Fast-Charging Lithium-Ion Batteries. *J. Am. Chem. Soc.* **2014**, *136*, 5039−5046.
(33) Muto, S.; Tatsumi, K. Detection of Local Chemical States of Lithium and Their Spatial Mapping by Scanning Transmission Electron Microscopy, Electron Energy-Loss Spectroscopy and Hyperspectral Image Analysis. *Microscopy* **2017**, *66*, 39−49.
(34) Huang, W.; Wang, J.; Braun, M. R.; Zhang, Z.; Li, Y.; Boyle, D. T.; McIntyre, P. C.; Cui, Y. Dynamic Structure and Chemistry of the Silicon Solid-Electrolyte Interphase Visualized by Cryogenic Electron Microscopy. *Matter* **2019**, *1*, 1232−1245.
(35) Zachman, M. J.; Tu, Z.; Choudhury, S.; Archer, L. A.; Kourkoutis, L. F. Cryo-STEM Mapping of Solid−Liquid Interfaces and Dendrites in Lithium-Metal Batteries. *Nature* **2018**, *560*, 345−349.

https://doi.org/10.1021/acsami.1c05966
ACS Appl. Mater. Interfaces 2021, 13, 34064−34073